Comprehensive Road Blockage Estimation for Urban Resilience with Artificial Intelligence Support

Graduate School of Engineering
(Civil Engineering)

Dilyara Akimzhanova 201889008

2025

Table of Contents

Abstract

This thesis explores road blockage detection during earthquakes, using GIS and AI to assess road accessibility and identify rubbles caused by collapsing buildings. The study incorporates buildings and rubble into a framework to develop a model for detecting and analyzing structural failures after earthquakes.

Past researches done in this field oversimplify reality and they do not account for spatial layout and most of them focus on building vulnerability rather than road blockages. Moreover, studies are data-hungry and can not be generalized. Therefore, this thesis aims to incorporate buildings and rubble into framework to build a model that will be able to detect and analyze the building collapse after the earthquake.

The study utilized satellite images taken before and after earthquake for cities of Antakya and Kahramanmaras. Images were annotated in ArcGIS Pro and were transformed to black and white to export and further use them in deep learning model. As the number of images was insufficient data augmentation was applied to artificially increase it. To allow model to learn both the presence and absence of collapsed structures background patches were added, and the Dice coefficient was used to assess segmentation quality, accounting for both positive and negative outcomes.

With the help of ArcGIS and AI, the model achieved a detection accuracy of 0.9319 for the training set, 0.6913 for the validation set, and 0.4982 for the test set. The limitations of the study include insufficient number of images and mountainous characteristics of the Kahramanmaras that resulted in decrease of test accuracy.

The research highlights the importance of road connectivity for social functionality and the challenges urban areas face during natural disasters. These insights can help improve emergency response plans and urban planning strategies, ultimately making cities safer and more accessible in the aftermath of earthquakes.

Chapter 1 - Introduction

1.1 Overview

Roads are critical in earthquake-prone locations since they are the first to be utilized after disasters. However, earthquakes may cause road networks to become impassable, creating delays in post-earthquake rescue efforts. Researchers investigated the vulnerability and obstruction of roads caused by earthquakes in order to develop contingency plans and execute seismic retrofits.

Past earthquake events have demonstrated that road damage can arise from both direct impacts, such as liquefaction and pavement cracking, and indirect impacts, primarily caused by building collapses. Previous scholarly works on the prediction of debris falling distance from building footprints have been classified into four distinct categories: methods with remote sensing monitoring, omnidirectional buffer-debris models, probabilistic and statistical models, and geometrical models.

The technology used by remote sensing monitors utilizes superior-quality satellite data and aerial pictures to detect road obstructions. However, this particular approach is not easily accessible for places that have not experienced recent earthquakes. The omnidirectional buffer-debris model predicts that debris resulting from the collapse of structures exhibits equal distribution across all directions, hence creating a buffer zone around the building where debris may potentially descend. Nevertheless, this particular model yields imprecise outcomes as a consequence of the arbitrary assessment of the buffer region. In order to study the frequency distribution of road blockages, probabilistic and statistical models use observed data and field surveys (Yu & Gardoni, 2022). Argyroudis et al. (2006) first introduced geometrical models as a solution to address the scarcity of observable data from previous seismic occurrences. However, these models are unable to distinguish the rubble production capacity of various structure types and damage conditions.

Positive models have also been employed in the estimation of road blockage probability resulting from building damage. However, these models are subject to two prevalent limitations. Firstly, they fail to account for the influence of road design on the road's capacity to accommodate vehicles. Secondly, they make arbitrary assumptions regarding the probability distribution used to estimate the probability of road blockage. This constraint hinders the

generalizability of models to many locations and has the potential to provide imprecise outcomes as a consequence of the presumed probability distribution function (Yu & Gardoni, 2022).

The document encompasses the primary concepts for the study, methodology, and the outcomes of the thesis. This thesis provides an overview of road blockage estimation during earthquakes, with a specific focus on rubble formation scenarios. Various approaches are used to assess road accessibility during earthquakes, including geographic information systems (GIS) and artificial intelligence (AI). The primary goal of this thesis is to detect road blockages due to collapsing structures after earthquakes. For this purpose, buildings and rubble will be incorporated into framework to build a model that will be able to detect and analyze the building collapse after the earthquake. This model will be generalized for different scenarios of building collapse and road blockage.

This study revolves around Road Blockage Estimation (RBE) and its importance in urban resilience. It emphasizes the necessity of road connection for social functionality and vulnerability to catastrophes such as earthquakes. The thesis investigates existing approaches for forecasting debris falling distance, including graph and percolation theories. The objective is to detect rubble formations that may potentially block road accessibility. By doing so, study aims to create a more comprehensive understanding of the potential obstacles and challenges that may arise in urban areas during natural disasters or other emergencies. This information can then be used to develop more effective emergency response plans and strategies to improve overall safety and accessibility in urban environments.

1.2. Thesis Statement

Roadblocks brought on by building collapse after earthquakes pose significant difficulties for disaster management and emergency response. The goal of this project is to create a system that can detect and evaluate these obstructions using Geographic Information Systems (GIS) and Artificial Intelligence (AI). The framework can detect buildings that have fallen and determine how they affect neighboring roadways by fusing satellite imagery with AI models such as UNet and UNet++. ArcGIS is also used in the study to produce maps and other visual aids that aid planners in making prompt and efficient decisions. The effectiveness of this technology in various urban settings will be evaluated through case studies of recent earthquakes in Turkey. In

addition to addressing typical issues like data limits and model correctness, this study demonstrates how this strategy might aid in disaster preparedness and urban planning.

1.3. Objectives

The main objectives of the research are

- Determine key parameters that contribute to the building collapse;
- Implement satellite imagery in ArcGIS Pro to detect and categorize road blockages both before and after seismic events;
- Develop a model that integrates ArcGIS Pro and AI for detecting building collapse after earthquakes;
- Automate the identification of rubble and debris using AI;
- Evaluate the accuracy and efficiency of the model in recognizing collapsed buildings and rubble from satellite images;
- Enhance the efficacy of emergency response plans and tactics in order to improve safety and accessibility within urban settings.

Chapter 2 - Literature Review

2.1 Parameters and predictors of building collapse

A structure's collapse after an earthquake is due to structural system integrity breakdown due to excessive deformation or force demand. This can lead to the collapse of the structure in part or entirely. Two types of collapse are most likely: sidesway collapse and vertical collapse. Primary one occurs when structural components lose their load-carrying capability, allowing second-order effects to overcome gravity load resistance. As regards latter collapse, it occurs when structural components lose their capacity to support gravity loads (Zareian et al., 2010).

For long years, the industry has given minimal consideration to collapse prediction. The fundamental explanation for this might be that elastic design principles prioritize comfort above collapse safety. Good detailed standards, insufficient attention to capacity design ideas, and constraints on maximum permitted storey drifts are seen to be acceptable. This has several benefits and is still widely used today. In the 1990s, there was a lack of understanding of how degradation in component strength and stiffness affects structural response (redistribution of internal forces). This led to attempts to gain a better grasp of behavior at deformation levels where components and elements are expected to fall apart (Krawinkler & Zareian, 2007).

The failure of roadside structures is the most prevalent reason for urban road network obstruction following large-scale earthquakes. Previous big earthquakes, such as the 2023 Turkey earthquake, have resulted in numerous instances of route blockages. Building collapse may drastically prolong emergency response time, necessitating the establishment of a road network rehabilitation framework, particularly in densely populated areas with low building standards (Hosseini et al., 2024).

The categorization of building typology is determined by both the anticipated factors that impact the seismic performance of the building and the availability of data (Spence et al., 2007).

The categorization of buildings may be significantly influenced by the specification of the year or era of construction, since building methods have evolved throughout time. The earthquake resistance of contemporary designed buildings is expected to be significantly influenced by various factors related to the construction form, including the presence of a "moment resisting frame" or "shear wall" in concrete-reinforced structures, as well as the number of floors (Spence et al., 2007). The correlation between the probability of earthquake-induced

destruction and the height and age of a structure is well acknowledged. Both of these variables are used, in either the direct or indirect manner, in the calculation of damage resilience metrics. Hence, the inclusion of these two architectural features as predictor variables is warranted (Mangalathu et al., 2020).

The form or configuration is a crucial factor that influences building reaction. The seismic activity of a basic rectangular building produces a reasonably consistent allocation of forces across the structure. Forces intensify at the interior corners of a more sophisticated T or L shaped structure (see Figure 1) (Tung, 2004).

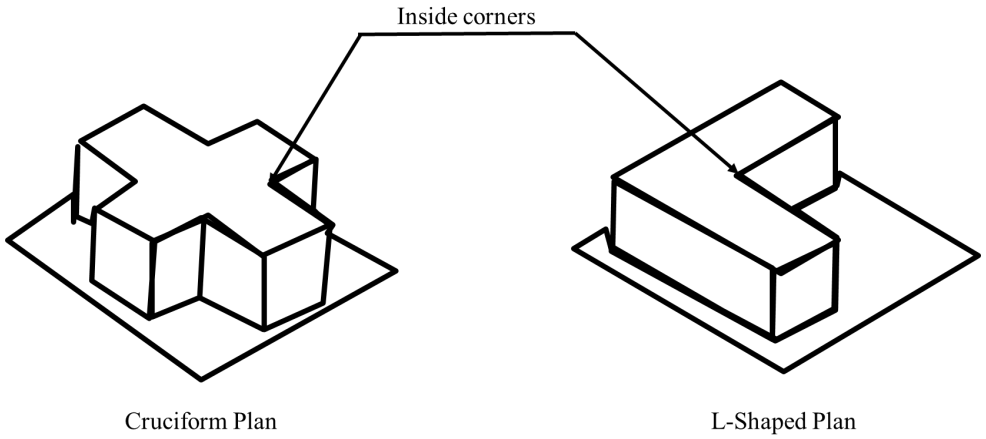

Figure 1. Examples of buildings with irregular configurations (Tung, 2004)

Another essential feature is the basic period of oscillation of the structural element (which is expressed in seconds). Their basic period is complicated and relies on the structural system's strength, weight, and overall height. Seismic impulses with identical periods may produce resonance, increasing the strength of the seismic forces that the element must withstand (Tung, 2004).

Numerous more factors pertaining to the building of structures have been demonstrated to have an impact on their seismic vulnerability that includes planar and vertical irregularities, foundation type, and quality of the building. Nevertheless, acquiring precise quantitative measurements of the distinct impact of these elements is challenging, and it is presumed that they are included in the range of anticipated harm within each category (Spence et al., 2007).

2.2 Factors affecting the probability of road blockage

The chance of traffic obstruction is determined by three elements. The primary determinant is the road's capacity, denoted as C, to handle debris while facilitating the passage of emergency vehicles. The value of C is contingent upon the width of road elements, such as vehicle lanes, sidewalks, on-street parking, and raised traffic medians that serve as barriers between lanes. Additionally, the usability of elements that are not obstructed by debris, such as vehicle lanes, or their unusability, such as specific sidewalks, on-street parking, and traffic medians, also plays a role in determining C (Yu & Gardoni, 2022). The seismic forces result in the failure of vulnerable slopes. This kind of damage is often seen in regions characterized by mountains or hills. Another kind of traffic obstruction occurs in metropolitan settings. Debris from several fallen structures, such as houses and electric posts, descends into the road. Just like a landslide, the road structure exhibits little damage, with just minor alterations on the road surface. Vehicles are unable to traverse the road because the route incurs both physical and functional damage due to the destruction of several infrastructural pieces (Tung, 2004).

The debris distance, Db, is the second element that influences road congestion. The obstruction of a road may occur when the distance of debris exceeds the minimum width necessary for an emergency vehicle. A road is considered unobstructed when it has sufficient capacity to handle waste and facilitate the passage of emergency vehicles. Db is determined by the building's features, including its dimensions (height, width, and length) and the kinds of structural and non-structural components included in the structure (Yu & Gardoni, 2022). In some cases when the earthquake magnitude is low or moderate, the road may be repurposed provided that the debris is eliminated so that it returns its capacity (Tung, 2004).

The third consideration pertains to the seismic vulnerability of the structure. Buildings that are more susceptible to deterioration are more prone to producing debris from both the structural and non-structural components. Extensive research has been conducted on the likelihood of building damage based on specific measures of hazard severity, using fragility functions. As an example, Gardoni et al. suggested a methodology based on physics to create fragility functions for structures. The methodology first formulated probabilistic capacity and demand models from laboratory data or field observations. The limit-state function is defined using probabilistic capacity and demand models, and fragility functions are derived by extensive reliability evaluation. Frailty functions are mathematical expressions that represent the

conditional likelihood of achieving or surpassing a predetermined level of performance, based on a measure of danger severity. After establishing the fragility functions for a particular kind of structure, the conditional probability of the building can be determined being in a certain state of damage by comparing the fragility curves. Given the extensive development of the technique in previous research, this study does not provide any new contributions and instead relies on the current approaches (Yu & Gardoni, 2022).

In accordance with United Nations definitions (1991), vulnerability is an extent of loss to a component at risk caused by an incident of a natural phenomena, measured on a scale of 0 to 1.

The predicted magnitude of particular damage to the physical infrastructure under a certain degree of hazard is represented by the infrastructure's real vulnerability (Davidson, 1997). In general, a damage ratio—which is the repair cost divided by the replacement cost—is used to quantify the extent of structural damage, and a vulnerability curve, also called a fragility curve, is used to illustrate structural vulnerability (see Figure 2) (Tung, 2004).

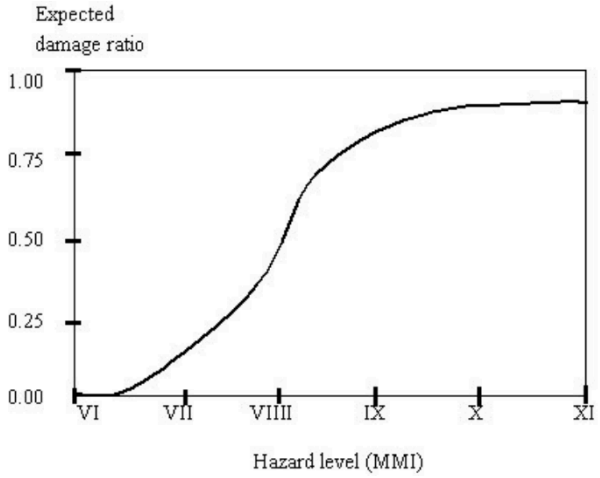

Figure 2. Damage curve (Tung, 2004)

A damage curve shows the expected degree of injury depending on the level of risk. The particular structures' vulnerability may be examined using criterion analysis principles (see Figure 3). The ultimate vulnerability of a system might thus be regarded as the total of the vulnerability based on each criteria (Tung, 2004).

Road
Location
Structure
Design code
Physical condition
Distance to structures (buildings, posts, electricity lines, overpasses) and the vulnerability of those elements. Embankment height Position (on ground level, or elevated, overpasses…
Age
Material

Figure 3. Criteria for vulnerability assessment of roads (Tung, 2004)

2.3 Earthquake damage measures and urban network restoration

Types of roads that are often seen in both urban and rural areas may use the suggested scale presented by Anbazhagan et al. (2012). The state of the roads and their capacity for post-earthquake relief efforts inform the recommended damage scales for roads.

Roads that are in acceptable condition and just need minor repairs are represented by the first scale. This category is appropriate for post-earthquake relief efforts and is easily accessible.

Less damaged roads are represented by the second scale, which may include mild cracks and side, shoulder, and footpath collapse. These roads need mild to moderate repairs, but they are accessible.

The third scale denotes significant damage caused by liquefaction, landslides, and other consequences of earthquakes to roadways with large fissures. These roads need moderate to extensive repair or cleaning because they are partly obstructed by land slides, buildings collapsing, storm surges, and tsunamis.

The fourth scale shows significant damage to highways, rendering them partially impassable. Large cracks, pavement layer failure, large holes, and extensive damage on one side of the road fall under this category. These roads need significant maintenance and rehabilitation in some areas and are obstructed by landslides, building collapses, storm surges, and tsunamis.

The highest grade, the fifth, indicates very severe damage to roadways near an earthquake's epicenter, leaving them impassable and unusable. This is because of the high

earthquake magnitudes, close proximity to epicenters, and total breakdown of the asphalt's top layer and sublayers as a result of liquefaction and landslide.

The two types of network obstructing model and emergency post-earthquake recovery schedule studies are as follows: the first one is concerned with building failure simulation and blockage likelihood in the absence of a recovery plan, while the other is more concerned with network recovery schemes. In order to mimic road obstruction, these studies — which are often carried out in Operations Research and Management Science (OR/MS) — never include seismic simulation of building collapse. Both issues should be taken into account concurrently in a workable solution. Mathematical restoration models are introduced in OR/MS research via the use of graph theory, network modeling, and linear/dynamic programming approaches. Recovery schedules are optimized using objective criteria such as traffic flow, capacity, centrality, accessibility, and distance traveled. Certain studies evaluate the road network's susceptibility only based on restoration plans, which might be helpful for evaluating the network's performance after an earthquake (Hossein et al., 2023).

Numerous research works have created probabilistic frameworks to evaluate the emergency response functionality of metropolitan road networks in the event of a seismic hazard. These frameworks take into account many criteria, including serviceability, accessibility, and network traffic demand. In high seismicity zones, these studies have also included connection reliability as a performance metric during the emergency response phase. This research uses the probability distributions of debris volume and resource removal rate to compute the anticipated value of route emergency restoration time, or opening time (Hossein et al., 2023.

The repair of urban roads after a severe earthquake can be divided into two critical stages: the Emergency Response Phase (ERP) and the Comprehensive Recovery Phase (CRP). During the ERP, the primary goal is to provide immediate relief and evacuate people, with the focus on clearing blocked roads to allow rescue vehicles and emergency services to pass. This phase can be planned more efficiently by estimating possible structural damages and rubble formation scenarios in advance, as they impact road accessibility and debris clearance operations. During the CRP, the attention shifts towards the comprehensive recovery of the transport system to normal operating circumstances. The main focus is on assessing and developing a resilient connection between the road network and strategically allocating resources for long-term reconstruction. Restoration time is heavily influenced by limited available

resources and the unpredictable nature of debris clearance volumes during the disaster response phase, which is the main source of uncertainty in network recovery (Hosseini et al., 2023). Developing potential structural damage and rubble blockage scenarios before emergency situations can provide effective support during the CRP as well. However, predicting road closures due to possible collapsing structures remains challenging due to considerable uncertainty surrounding the volume of debris and the time required for clearance.

2.4 Opportunities for ArcGIS and AI Integration in Road Blockage Estimation

Yoshinari et al. (2017) describes a method for identifying collapsed buildings by estimating the quantity of debris using aerial photos taken during a catastrophe. They extract straight lines from aerial photos, presuming that lines represent building roofs, in order to identify collapsed buildings. The subject of this thesis is about roofing on houses. Maps of homes often include aerial pictures of their roofs. The overhead view can reveal a different roof or no roof at all if the target house falls. Damage identification may be aided by roof condition. They then used the recommended method to real aerial photos that were obtained in affected locations soon after the Great East Japan earthquake. The proposed approach properly approximated the quantities of debris left behind after a catastrophe when compared to current methods. Before the system can be put to use in real-world scenarios, its capacity to extract roof features has to be strengthened.

The Karmania Hazard Model, a GIS-based model, is used for database storage, querying, and analysis. Its interactive interface allows users to process data, equations, and computations quickly. This study suggests that GIS-based scenario planning is a useful tactic for managing seismic crises before, during, and after an earthquake. GIS, proper data processing, standard equations, and precise data sources provide reliable seismic simulation results. The quality of data input and connections between geographical data layers affect the output of simulation modeling. The model was tested during the 2003 Bam City earthquake, producing building and population maps, ground shaking maps, and seismic microzonation maps. These maps enable urban planners to create new and amend plans, prioritize building reinforcement plans, and develop educational programs to better prepare people for disasters. The Karmania Hazard Model's suitability and effectiveness in disaster management stages include resource estimation, preparedness, and hazard mitigation (Hassanzadeh et al., 2013).

Convolutional neural networks (CNNs) have been a major research issue for speech analysis and image recognition in recent years. Forrest Iandola's SqueezeNet is another CNN example that can attain ImageNet accuracy on par with AlexNet's. Complete building collapses are readily identified from VHR photos due to the textural characteristics of the damaged roof components. Because the damage effects are mostly shown along the facade, which is not visible in this kind of picture, lower damage classes are more challenging to map (Ji et al., 2018).

With an emphasis on the 2010 Haiti Earthquake, Ji et al. (2018) explore the use of CNNs, notably SqueezeNet, using post-earthquake VHR satellite images to detect collapsed structures. Three balancing techniques—random under-sampling, random over-sampling, and cost-sensitive approaches—were used to improve the accuracy of identifying collapsed structures. QuickBird satellite images captured after the seismic event. According to the given rules, the building damage level was classified into five categories: G1: Minimal damage, G5: Complete destruction, G4: Extremely heavy damage, G3: Substantial damage, and G2: Moderate damage. Additionally, the study region's building footprints were manually extracted using ArcGIS 10.4. After that, the study area was split into three zones: test A, test B, and train. The results demonstrated how useful post-event imaging is for gathering information on building collapses. SqueezeNet performed well in differentiating between buildings that had collapsed and those that were still intact, averaging an overall Accuracy of 78.6% over the two test locations. With the use of the cost-sensitive strategy, the average Kappa value rose from 41.6% to 44.8% after the balancing measures.

The paper by Hansapinyo et al. (2020) presents a novel approach for forecasting urban building damage using the adaptive neuro-fuzzy inference system (ANFIS) model. The research process involved assessing various earthquake damage scenarios using the capacity spectrum method (CSM). An ANFIS model was created and trained using building damage datasets. Building damage estimates from the CSM and the ANFIS model were compared under five different scenarios. The ANFIS model was found to be the most accurate for forecasting building damage with a single depth, location, and different magnitudes after thirty-two models were trained. The ANFIS model offers two main benefits: it allows fuzzy logic functions to handle input uncertainties and can be adjusted with more precise training datasets. It also leverages machine learning through the neural network system, making it suitable for low to moderate earthquake-prone cities.

Another research used three different CNN models—composite, twin, and fusion—to pinpoint four different categories of damage that resulted from the 2016 Kumamoto earthquake. The specific objectives were to design experiments using three CNN models for building damage identification from orthophoto images, evaluate the performance of the proposed models, and investigate the impact of CNN architecture on accuracy. The RGB (red, green, and blue) photos taken both before and after the main shock of the 2016 Kumamoto, Japan earthquake were selected as the research region. Four classifications were considered in this study: (i) no damage, (ii) little damage, (iii) debris, and (iv) backdrop. The RGB form photos of the major shock event (before and after) were used to identify the damaged structures in the present research. The damage detection procedure was executed by three separate models, each of which used a unique CNN structure with numerous layers to mimic the operation of the human brain. The results showed that the damage detection paired model had an overall accuracy of 76.85. The proposed framework showed suitability in recognizing building damage from RGB photos overall. Interestingly, the CNN models showed acceptable accuracy even without the additional layer of complexity created by using elevation data in the study location (Kalantar et al., 2020).

Another useful way is to integrate Machine Learning with Geographic Information Systems (GIS) and Remote Sensing (RS) which will improve the prediction of building collapse and road blockage after earthquakes. ML techniques introduced by Liu et al. (2022) like supervised classification, unsupervised learning, and deep learning (e.g., CNNs) can automatically detect collapsed buildings from satellite images and estimate the severity of road blockages. Data fusion from several sources, such as optical and radar imagery, maximize the accuracy of damage assessment by showing a detailed and different view of the affected areas (Liu et al., 2022). Real-time data from sensors and drones can further improve these predictions which will affect quicker disaster response (Liu et al., 2022). But in this case difficulties such as data quality, computational complexity, and the need for large labeled datasets must be addressed (Liu et al., 2022). Moreover, ML models should be able to utilize more interpretable techniques in the form of AI (XAI). Therefore, its integration with GIS and RS can significantly enhance disaster management and recovery efforts.

Moreover, Yu et al. (2024) explores the the use of ML to assess the urban roads during disasters in Hangzhou's Binjiang District. The authors provide a comprehensive approach that integrates field data with ML techniques, particularly XGBoost model that can predict road

collapses. The research fill the gap by expanding the data points and optimizing the dataset parrtitioning going beyond traditional methods that often fail to mention imbalance dataset issues. They use various factors including soil layers, groundwater richness, and human activity that improve the accuracy. Additionally, SHapley Additive exPlanations (SHAP) is utilized to show the predictions of ML methodology that improve the decision-making process.

2.5 Calculation of road blockage level

Earthquake-related hazards pose both direct and indirect dangers to city roadways. Suspended constructions, such as bridges or overpasses, are particularly susceptible, although tunnels may also be damaged (Franchin et al., 2011). Another source of worry is structural degeneration over time. Topology and regional soil influences may have an impact on ground-level road sections, causing partial or total interruption. Flooding, tsunamis, accidents, and explosions may all be serious consequences of an earthquake (Kawashima & Matsuzaki, 2012).

A collapse of a structure may restrict traffic flow on roads owing to debris, emergency, and recovery efforts. As people throng the streets following an earthquake, unexpected traffic patterns emerge, resulting in higher car crashes. Public transportation may be unavailable for a certain time, and rescue vehicles from a variety of agencies, including firemen, paramedics, police, construction trucks, military personnel, and utility distributors, might cause roadblocks (Toma-Danila, 2018).

Inventory assessment is critical for mitigating these hazards. Geographic information systems (GIS) serve to manage geographic data, model transportation systems, and represent inter- and intra-component connections. ArcGIS is the most sophisticated GIS system for roadway modeling, although it does not provide dynamic traffic simulations. Road network GIS data may be acquired from a variety of sources such as national records, publicly or privately accessible data, and the OpenStreetMap Project, which offers free, generally accurate, and up-to-date GIS road network vector data. Contributing to and using this program is suggested (Toma-Danila, 2018). A GIS, an interdisciplinary geospatial platform, brings together scenario-based spatial analytic tools such as disaster simulation, impact assessment, crisis management, and natural disaster mitigation tactics. GIS-based spatial decision-making systems are proven to aid in studying and predicting future hazards, including earthquakes (Feizizadeh,

2023). By utilizing it the probabilities of building collapse based on certain relevant parameters (e.g., building height, shops, age of construction) may be calculated and an earthquake simulator can be made. This simulator will create the polygons (rubble area) and status (collapsed or not collapsed) for a given map.

Traffic data is critical for simulating the issues caused by network traffic and human activities. However, gathering this information may be difficult, but new data collection methods, such as crowd-sourced smartphone data or electronic sensors, make it simpler for large corporations to include current or historical traffic maps and services. National authorities are also responsible for keeping tabs on traffic, and certain data may be acquired from them (Toma-Danila, 2018).

To quantify the impact of earthquake hazards on transportation systems, structural components must be assessed for vulnerability, as well as seismic hazard and local site impacts. The suggested technique adds a new characteristic to the conventional defining schema of road segments: the likelihood of roadways being impractical in the event of an earthquake. This chance may be estimated using a variety of factors, including structural collapse, obstruction due to construction debris, or traffic. Expert judgment, remote sensing, and empirical formulae may also be employed. Fragility curves may help quantify this risk (Toma-Danila, 2018).

The following term may be used to represent the quantity of debris blocking the roads: Road blockage level = Density of collapsed buildings + Building characteristics + Relative distance between roads and collapsed buildings (Tung, 2004).

The form of construction is also considered. The type of building was taken into account even while estimating the number of collapsed structures. But the shapes of the rubble or collapse vary depending on the kind of structure (Tung, 2004).

Only homogeneous units made up of those buildings are chosen because only the debris from fallen buildings that are near to and directly front the road may have the potential to obstruct it (Tung, 2004)

2.5.1 Density of collapsed buildings

One element influencing how much of a road segment will be blocked by debris or what proportion of the road segment will be impacted by the debris is the density of fallen buildings along the route. The number of collapsed buildings per homogeneous unit, which is derived from

Guragain's (2004) building vulnerability assessment study, may be used to determine this density (Tung, 2004).

The plan area A_c occupied by the collapsed buildings based on information about the number of buildings in a homogeneous region and the overall number of buildings in the same unit.

$$A_c = \frac{N_{cb}}{N_b} A_b$$

Where:

N_{cb}: The quantity of crumbling structures per unit of homogeneity

N_b: The total number of structures (based on the footprint map) each homogeneous unit.

A_b: The whole building area in the homogeneous unit, as determined by the footprint map.

The ratio between the area of the complete homogeneous unit and the collapsed regions is determined to get the "collapse density by area".

$$P_A = \frac{A_c}{A_{unit}}$$

Where: an area of a homogeneous unit is called an A_{unit}.

The "linear collapse density" for a given homogeneous unit may be determined using the "collapse density by area" in the following way:

$$P_L = k\sqrt{P_A}$$

Where: P_L: linear collapse density, which is the number of collapsed buildings per unit length.

k: a factor that considers the relative comparison between the building density within the homogeneous unit and the building density along the road.

Density outside the road is lower than that within (k=0.9). Density along the road is the same as inside in k=1.0, somewhat higher than inside in k=1.1, and much greater than inside in k=1.2.

The selection of the k value is contingent upon each distinct homogeneous unit. The footprint map shows how buildings are distributed inside a homogeneous unit.

This kind of blockage is known as longitudinal blockage as the evaluation is based on the likelihood that a portion of the road segment will be obstructed by debris and is expressed as a percentage of the road segment (Tung, 2004).

2.5.2 The distance between the road and the buildings

Structure to road distance has a major influence on the likelihood of a traffic obstruction. Road blockages are less likely to occur over farther distances. This also holds true for the separation between buildings on opposing sides of the road. The distance is called the difference in distance (D_B). In the event of a post-earthquake situation, D_B may be calculated using road width (W_R), high-resolution photos, or footprint maps. It can also be measured directly from the field. At the same road segment, the distance is taken to be proportionate to the width of the road (Tung, 2004).

$$D_B = \gamma \times W_R$$

2.5.3 Building characteristics

2.5.3.1 Material

The building's structure and material type has an impact on the assessment of the likelihood of a traffic impediment. Masonry structures like adobe, brick-mud, and brick-cement are prone to fall vertically, avoiding debris from distancing itself from the building layout. Stiff buildings, conversely, such as those made of steel and reinforced concrete, lean toward and fall to one side, moving the debris farther away from the initial construction's location. As a result, there is a greater chance of the debris pile growing and the road being blocked. As a result, the material-based factor M for RCC buildings is given a value of 1.3, while it is 1.1 for other material types (Tung, 2004).

2.5.3.2 Height

The average storey number of buildings along roads is calculated using the formula:

$$Height = 0.01 \times \Sigma Percentage\ of\ building.type_i \times No\ of\ storey$$

For instance, a homogenous structure with 50% 1-storey adobe buildings, 30% 3-storey cement- brick buildings, and 20% 4-storey reinforced concrete buildings would have an average height of 2.2 storeys:

$$H_E = 0.5 \times 1 + 0.3 \times 3 + 0.2 \times 4 = 2.2\ storey$$

Building height, building type, and previous earthquake debris photographs are used to determine the width of rubble away from a structure. The height of the structure affects the average width of debris. Figure 4 is used to predict the shape of debris (Tung, 2004).

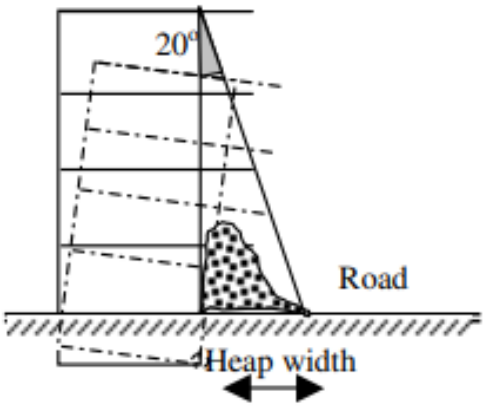

Figure 4. Estimation of debris (Tung, 2004)

An estimated 20 degrees separates the front wall of the structure from the line that extends from the roof to the most distant point of debris. The formula $W_D = H_E \times tan20$ is used to determine the width of the debris heap (Tung, 2004).

2.5.4 Final road blockage calculation

Based on the kind of building and the distance between the structures and the road, the blockage estimate attempts to estimate the likelihood that debris would block the road. This kind of obstruction is known as lateral blockage, and it is shown here, perpendicular to the center line of the road (Tung, 2004).

The ultimate width of the debris pile W_{FD} is computed as follows and is a function of M, C, and W_D:

$$W_{FD} = W_D \times M \times C$$

2.5.8 Other methods

By Mansouri et al. (2008) the road blockage index (RBI) is a tool used to assess the physical loss of buildings and the resulting bottleneck in the road network. It involves three steps: creating a city geodatabase and a GIS model, modeling structural vulnerability functions, and estimating the RBI. Phase one involves creating a city geodatabase and GIS model,

compiling data on seismic hazards, building inventories, transportation networks, and city geography.

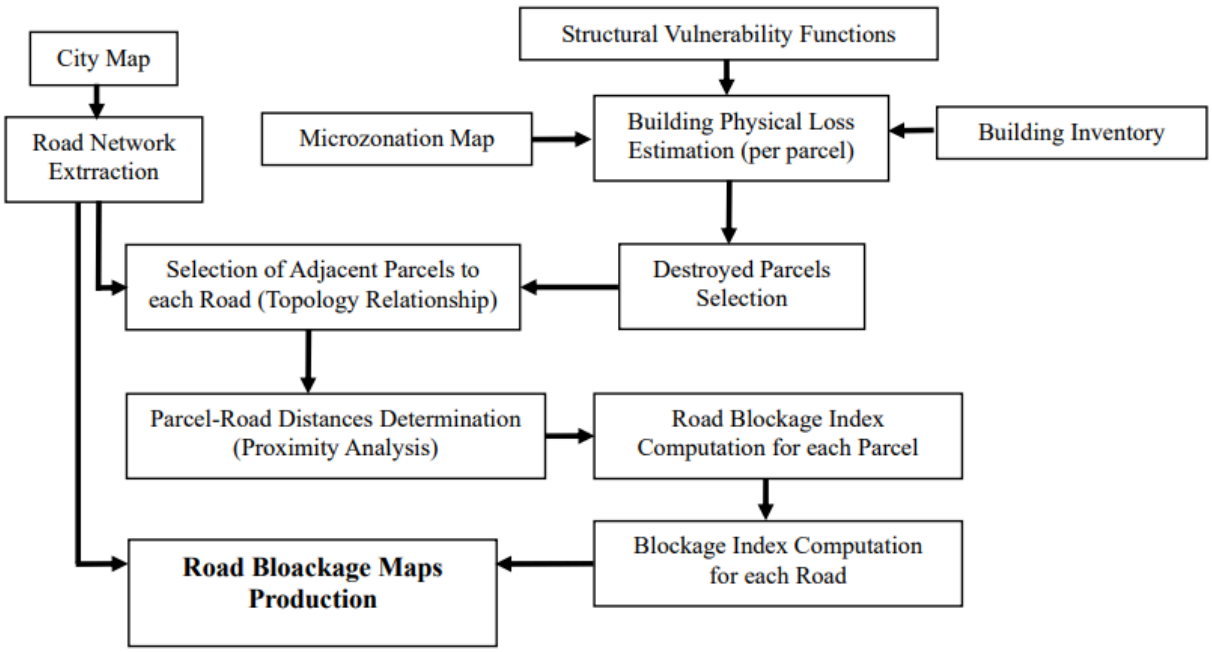

Figure 5. Flow diagram for steps in ArcGIS (Mansouri et al., 2008)

Phase two involves creating the road network obstruction index and modeling structural vulnerability functions, calculating building stock vulnerability for local circumstances. Phase three focuses on site-specific RBI estimates and GIS deployment, enabling 3D mapping of building stock and predicted levels of building damages. To produce 15 distinct patterns of building collapse, the number of buildings of each construction type was divided by a random number generator. Three tiers of road obstructions were established: full blockage, partly blocked roads, and completely blocked roads. The criteria for road blockage were based on a debris flow distance of 3 meters, as frontal flow is the worst possible direction for road blockages.

Damage mapping based on remote sensing is limited to the labor-intensive and time-consuming visual interpretation of optical satellite images. Damage-mapping research has used artificial intelligence (AI), but explainability is essential for practical uses. Explainable AI (XAI) models allow for problem-solving by providing insight into the causes and limitations of the model. In post-earthquake rapid damage mapping, when errors might result in fatalities, this is particularly important. A more reliable and comprehensible AI model may be developed by investigating the effects of AI inputs on output. An optical satellite image from the 2018

Palu/Indonesia earthquake is used in this study to train a multilayer perceptron model to extract image attributes and building footprints. According to the study, the identification of fallen structures in a study region is greatly impacted by spectral properties. Nevertheless, this may result in mistakes when implementing the concept in other regions. A training dataset that represents a variety of buildings and collapsed kinds is required to handle this. Additionally, by identifying training dataset restrictions that might provide biased findings, the work emphasizes the necessity of explainable AI for post-earthquake building-damage mapping (Matin & Pradhan, 2021).

A city-damage simulation model that shows the destruction of property due to a large earthquake is proposed in this study. The model was used to calculate the amount of property damage that would result from a fictitious earthquake that struck Tokyo's 23 wards. In addition to a ground-surface response model for structural failures, the model includes GIS data for estimating ground reaction for individual structures in the event of a large earthquake. It was found that buildings in the 23 wards of Tokyo had been built to withstand earthquakes (Hirokawa & Osaragi, 2016).

The development of a street-blockage estimation model showed that, even in regions with a low likelihood of building collapses, locations with a high likelihood of blocked streets are widely dispersed from east to west (Hirokawa & Osaragi, 2016).

When the micro-level fire-spread simulation model and the fire-spread cluster model were compared, it was found that by improving computation methods and computer speed, the micro-level fire spread simulation could be used over a large area (Hirokawa & Osaragi, 2016).

Additionally, the model added two additional indications of fire propagation: burnt-down potential and fire spread potential. Burnt-down potential is the chance that a building may catch fire, whereas fire-spread potential is the chance that adjacent structures will burn if no firefighting is done (Hirokawa & Osaragi, 2016).

structure collapse estimation is a crucial model, nonetheless, and it is preferable to have data on the age, seismic reinforcing design, and structural material of the structure. The purpose of the model was to gather basic data for simulation trials, such as shelter and firefighting after large earthquakes (Hirokawa & Osaragi, 2016).

In order to provide a technique for identifying structures that have fallen following an earthquake based on 3D geometric changes—specifically, height variations of the buildings the study done by Tong et al. (2016) uses pre- and post-seismic IKONOS stereo photo pairs.

The pre- and post-seismic IKONOS stereo pairs and enhanced 3D coordinates of the ground points may be used to identify each individual collapsed building by calculating the height difference of the structure's corner points. Additionally, the building's three states—completely collapsed, half collapsed, or not collapsed—may be determined, and the number of collapsed floors can be estimated.

The position of the fallen buildings may be determined by comparing the pre- and post-seismic DEMs generated from the pre- and post-seismic IKONOS stereo pairs. With an overall accuracy of more than 94%, collapsed structures may be identified using the difference DEM when the pixel and object-based assessment techniques are used.

2.6 Disaster Management

The four stages of disaster management are preparation, reaction, mitigation, and recovery (see Figure 6). By implementing construction rules and renovating infrastructure, one may avert future calamities and lessen their effects. Preparing ahead of time for a catastrophe in order to save lives and facilitate response efforts is known as preparedness. Response include carrying out previously created plans and tactics, including shelter management, emergency rescue operations, firefighting, evacuations, and humanitarian aid. In order to return functioning to typical, recovery includes repair and rebuilding activities such as debris removal, damage evaluation, and infrastructure restoration. Insurance firms and government organizations also contribute financially. All things considered, disaster management is an essential procedure for guaranteeing the security and welfare of people and communities in times of crisis. location. It relates to actions taken in advance of a catastrophe to support rescue and response efforts and preserve lives, including gathering water and food supplies, putting up emergency contacts, and planning evacuations. The reaction phase mostly implements the plans and tactics that have been created in advance. During a crisis, response operations take place. These often include searching and rescue missions, managing shelters, evacuating regions that are in danger, and providing humanitarian aid. The term "recovery phase" describes the period after a catastrophe when attempts are made to restore the area to its pre-disaster state or even higher. Reconstruction of the

infrastructure, exact damage assessment, debris removal, and financial support from governmental and insurance organizations are typical recovery measures (Sun et al., 2020).

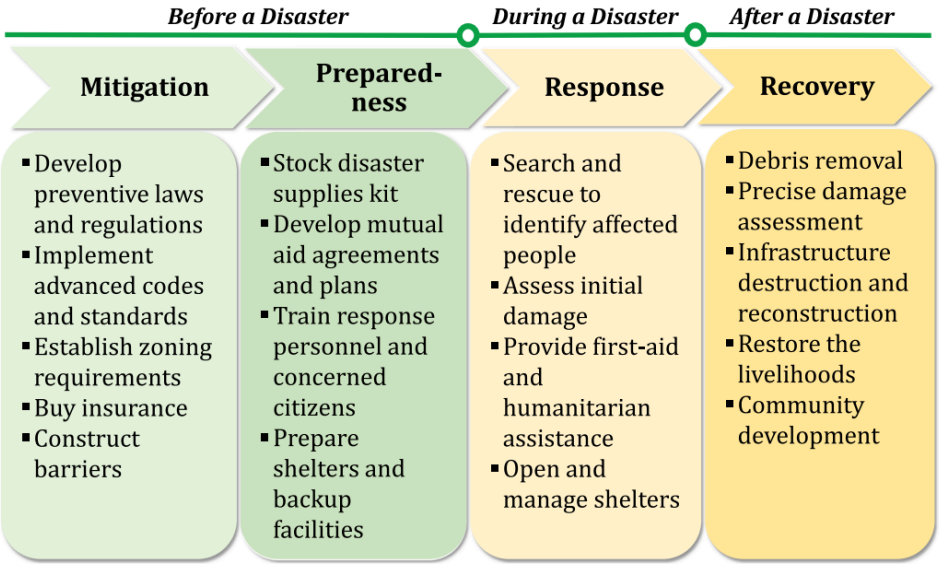

Figure 6. Disaster management stages (Sun et al., 2020)

Chapter 3 - Methodology

The study will follow the methodology steps below:

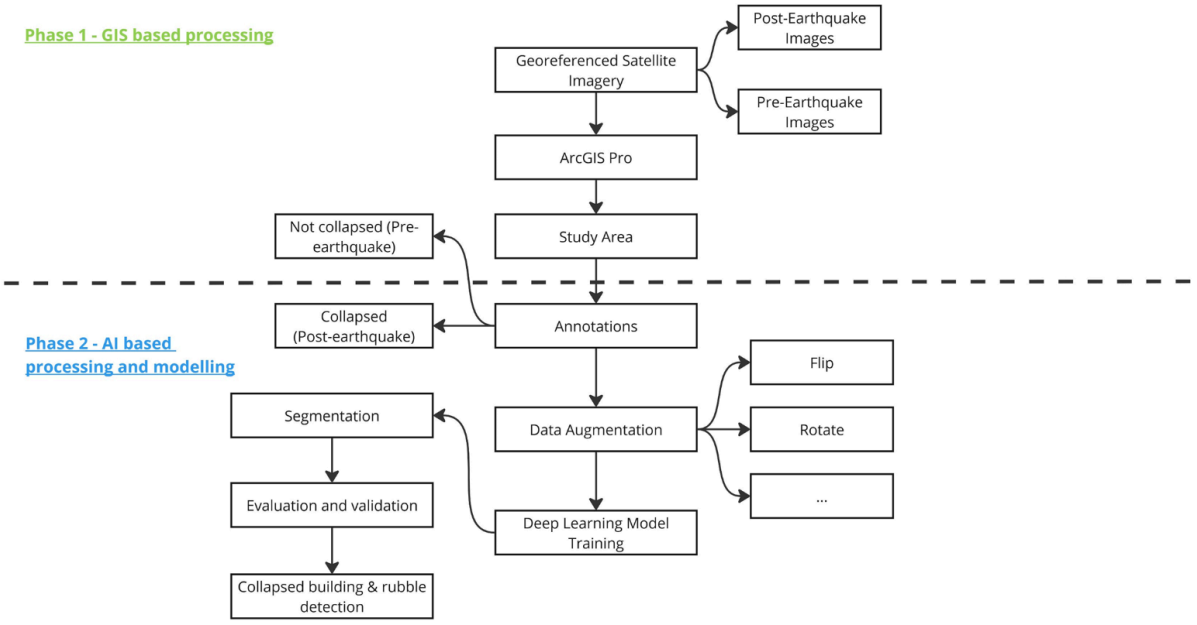

Figure 7. Methodology

The study used the Adam optimizer and Segmentation Models PyTorch library to train models for 30 epochs on a single NVIDIA Tesla V100-SXM3 GPU. The models were implemented using the SMP library, with SCSE attention modules incorporated for spatial and channel-wise feature recalibration. The input to the models was patches extracted from large-scale satellite images, with two different patch sizes considered. A sliding window approach was used to generate patches from high-resolution images, resulting in greater overlap between patches. Data augmentation techniques were employed to artificially expand the training data, with varying augmentation factors applied. To ensure the model could learn both the presence and absence of collapsed structures, a percentage of background patches was introduced into the training dataset. The Dice coefficient was used to evaluate model performance, accounting for both false positives and false negatives, providing a balanced assessment of segmentation quality.

3.1 Data pre-processing

Preparing the necessary information layers, such as high-resolution spatial satellite imagery taken both before and after the incident, is one of the pre-processing stages (Ranjbar et al., 2017). During the data processing phase, satellite imagery was gathered from reputable sources, such as public datasets and Maxar Technologies . In order to document changes brought about by the tragedy, these images featured both pre- and post-earthquake circumstances. After that, the images were cleaned and improved by enhancing clarity, reducing noise, and adjusting brightness.

The dataset was made more varied by applying data augmentation techniques including flipping, rotating, and brightness adjustment. By exposing the model to various iterations of the same data, this procedure enhanced the model's capacity for generalization. After that, the dataset was divided into training set, validation set and training set. The model was trained on the training set, its execution was followed throughout training on the validation set, and its execution on new data was evaluated on the testing set.

To make sure the images matched genuine places, geospatial alignment was done using GIS tools. This allowed the algorithm to produce predictions that matched real maps. To avoid bias in the model, techniques were employed to balance the dataset in situations when it was unbalanced, such as when there were more examples of buildings that had fallen than ones that were still intact.

Before the data was included in the model, it was carefully checked for errors and quality control throughout the entire process. The dataset's suitability for the analysis and modeling tasks was guaranteed by this preparation.

3.2 Annotation of collapsed buildings

Yoshinari et al. (2017) presents a technique for detecting collapsed structures using aerial images obtained after a disaster to estimate the amount of debris. To detect fallen structures in aerial shots, they extract straight lines (assuming they represent building roofs) from the images. This paper focuses on house roofs. Aerial photographs are commonly used to depict the roof of a home on a map. If the target home collapses, the aerial shot may show a different roof or no roof at all. Roof condition can help identify damage. Subsequently, they used the suggested approach to actual aerial pictures taken in affected areas shortly after the Great East Japan earthquake.

When compared to existing methodologies, suggested methods estimated disaster debris amounts more accurately. However, the system's ability to extract roof characteristics must improve before it can be used in practice.

Collapsed buildings are annotated based on the roofs using ArcGIS manually. The images were splitted to training, validation and test sets.

3.3 Data Augmentation

Based on the dataset provided data augmentation is utilized to make the detection process more generalized. As satellite images of one point may differ from one another by angle, quality and brightness. The common data augmentation processes include image rotation, adjusting brightness, vertical and horizontal flipping (Zou et al., 2024).

3.4 Deep Learning Model

Segmentation based deep learning model is utilized to detect the collapsed buildings and especially road blockages. During training satellite images consist of two colors, also they are called masked versions: white is for target objects (rubble) and the black is for the rest (Hacıefendioğlu et al., 2023):

Figure 8. Example of original and masked version of collapsed buildings (Hacıefendioğlu et al., 2023)

Deep learning methods have become more popular in the past years for picture segmentation, especially in emergency response and clinical imaging. The goal of semantic segmentation is to assign an object class to every pixel in an image; however, this is difficult since objects vary in dimensions, form, and position. Low-quality photos or occlusions present additional hurdles for disaster management solutions (Hacıefendioğlu et al., 2023).

Manually annotated buildings will act as masks and will help in identifying rubbles. This will provide quick emergency response as the system will automatically detect the blocked roads after receiving post earthquake satellite images.

3.5 Evaluation and Validation

After training the model it is tested for correct identification of rubbles. The proposed model should work on different earthquake scenarios including earthquakes in different cities.

Deep learning systems are consist of several mathematical operations or nodes grouped in a systematic way. The ability of the neural network to learn is crucial to its functionality since insufficient learning can lead to both overfitting and underfitting. To avoid these issues, learning capacity has to be appropriate for task complexity and data volume (Eelbode, 2021).

To verify a deep learning system's correctness on future unknown data, the concepts of training, validation, and testing must be applied. To do this, the dataset must be divided into three parts: the training set, which finds patterns in the images and labels; the validation set, which verifies if the model is overfitting or underfitting; and the test set, which offers an unbiased evaluation of the model's performance (Eelbode, 2021).

Sets must be unrelated to one another in order to avoid bias and ensure that the images in different sets are not connected. The "generalizability" argument would be strengthened if the test set were independently collected (Eelbode, 2021).

The amount of data needed depends on the task's difficulty, the kind of input data, the label's quality, and the desired performance. The ratio used for testing and validation should be big enough to capture the whole range of variability available in real life, while the remaining portion can be used for training. As data volume rises, this ratio will fall (Eelbode, 2021).

3.6 Algorithm Design

3.6.1. U-Net Architecture

Shahi (2024) explains the U-Net is a architecture that is based on Convolution Neural Network and designed for the semantic segmentation purposes. It contains both speed and the most accuracy among other types of architectures. Its structure build from two paths: encoder that catches the contextual data and a decoder that is made for precise localization. Both form a U-shaped arrangement.

Encoder is an important part as it accepts the input data and processes it despite it contains complex information, in this case it is satellite images. Encoder has a hierarchical structure which enables down sampling. It is crucial in terms of computational efficiency as it gives an opportunity to highlight only major features.

The bottleneck layer where encoder and decoder meet acts as a transitional point by conveying the main data that was produced during encoder phase in a condensed form. Decoder in its turn expands the given information.

Chapter 4 - Case Study

4.1 Study Area Selection

The study areas were chosen from Turkey: Antakya and Kahramanmaras cities that are located in active seismic zones. These locations were chosen because they reflect various metropolitan environments. Adıyaman has more rural parts, Kahramanmaraş has a mix of residential and industrial zones, while Antakya is known for its rural neighborhoods. This diversity makes it possible to evaluate the system in a range of settings. The 2023 earthquakes also had a major impact on several cities, resulting in major building collapses and road closures. They emphasize the need of creating trustworthy instruments for forecasting road obstructions in earthquake-prone areas because they are located close to important fault lines. Furthermore, because prompt traffic clearing is critical in regional emergency response networks, these cities are vital. By concentrating on these areas, the system is guaranteed to be evaluated in real-world scenarios and made flexible enough to be applied to other areas with comparable risks.

4.1.1 Antakya city

The research area is located in a very dynamic zone in the eastern Mediterranean region where the African, Arabian, and Eurasian plates converge, resulting in moderate to major earthquakes. Antakya is situated in south-east Turkey and has an inhabitants of around 150,000 people. The housing and population centers are located along the Asi River, which runs through Antakya in Samandag district, connecting Syria to the Mediterranean Sea (see Figure 9) (Över et al, 2011).

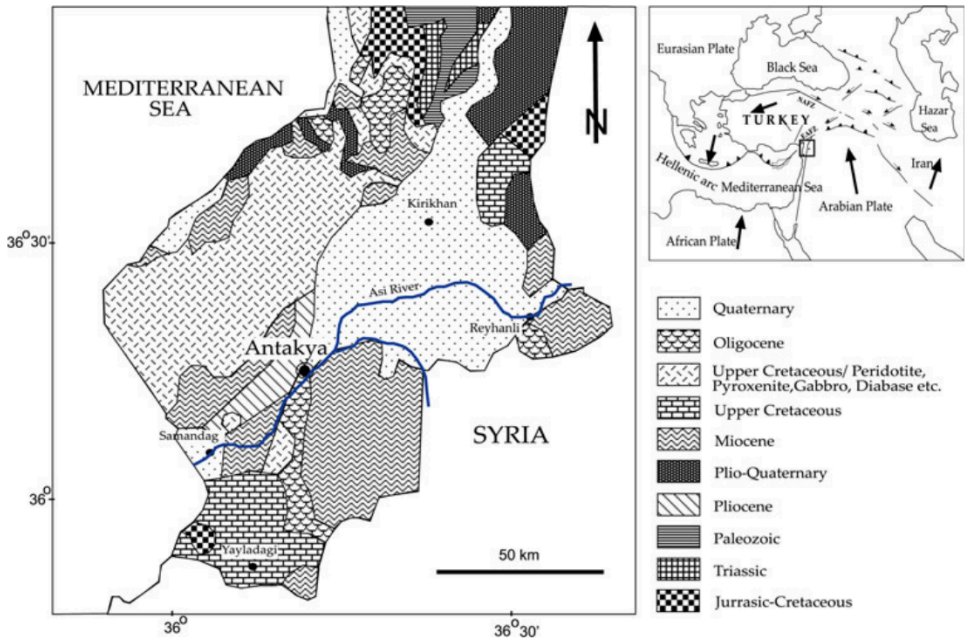

Figure 9. Geological map ofAntakya. Inset map shows the location and main tectonic units (Över et al, 2011)

Turkey's Antakya is renowned for being situated in an area with many geological formations and intense tectonic activity. The city is located where the Cyprus-Antakya, Karasu, and Dead Sea fault lines intersect, resulting in varying ground conditions within short distances. The Hatay Graben, which fell in the Cretaceous and Eocene eras and filled with saltwater in the Miocene and Pliocene eras, had an impact on the city's position. From a strike-slip faulty type to an extensional regime, the active stress regime has progressed, igniting prior fault lines and creating new ones. Numerous earthquakes have struck Antakya and the surrounding area, severely damaging property (Özşahin & Değerliyurt, 2013).

The qualities of geological materials underneath a place may have a significant influence on seismic activity. Past seismic events have demonstrated that harm is often larger on soft soils than on stiff soils and rock sites when the building is more than a few kilometers from the place of the earthquake's origin (Över et al, 2011).

4.1.2 Kahramanmaras city

Kahramanmaras Province is located on the Kahramanmaras Plain, which has alluviums formed by the Eastern Anatolian Fault and Miocene units south of Ahır Mountain. In the Kahramanmaras province, the settlement of Elbistan is encircled by undifferentiated continental

clastic rock in the north and east-west and limestone in the south. According to soil data, alluvial soil covers the majority of Adana's city center (Mertol et al., 2023).

Nonetheless, the city's northern regions have a travertine geological feature. Elazı g has the most varied soil types among the earthquake-affected cities, including alluvial, clastic and carbonate rock, and limestone. Other studies may provide a more thorough analysis of the city's soil and how it affects building (Mertol et al., 2023). Around 12 million years ago, during the Neotectonic period, plate movements were caused by continental drift, according to seismologists. Since the larger Arabian plate converges with the smaller Anatolian plate in a north-south axis, the displacement of these tectonic plates is the main cause of all major earthquakes in Turkey (Mertol et al., 2023).

The region where the African, Arabian, and Anatolian tectonic plates merge is where the Kahramanmaraş earthquakes struck. The Dead Sea Fault (DSF) zone, an extension of the East African Rift (EAF) zone that separates the African and Anatolian plates, is the area where the Arabian and African plates are continuous. Tectonic plate movements along the fault lines of these large contact surfaces cause significant earthquakes in the region (see Figure 10) (Mertol et al., 2023).

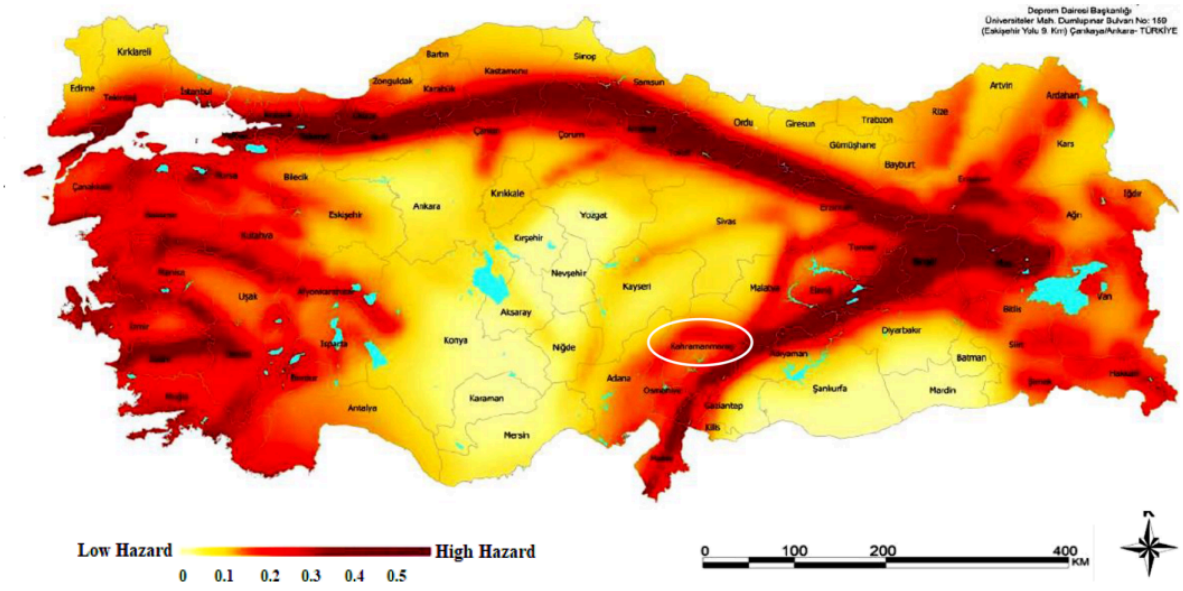

Figure 10. The Seismic Hazard Map of Turkey (GDDA 2019)

4.1.3 Adiyaman city

The location of Adiyaman province is 37° 45' 50" North latitude and 38° 16' 40" East longitude. The study was carried out in the central district of Adiyaman, which is an urban area. There are 33 neighborhoods in Adiyaman City as of 2023. The neighborhoods of Altinsehir to the west, Varlik to the south, Yunus Emre to the east, and Cumhuriyet to the north serve as the boundaries of the research area (Vural, 2024).

Ivanov & Chow (2023) inform that 92% of the population lives in temporary settlements, Hatay, Adiyaman, Kahramanmaras, and Malatya which are the areas most severely affected and have the highest PGA measured at the closest stations. PGA is the maximum ground acceleration experienced during an earthquake. It serves as a gauge for the intensity of seismic wave-induced ground shaking. The city of Adiyaman is situated in southeast Turkey, around 200 kilometers from the Syrian border. It acts as the district and province of Adiyaman's administrative center. With a population of 632 148, the mostly Kurdish city of Adiyaman was one of the areas most severely affected by the earthquake, with 8387 fatalities and 17499 injuries. According to the local authorities, 487 169 people live in tents and containers around the city of Adiyaman and the province, while 122 884 people left the province (Ivanov & Chow, 2023).

The city Adiyaman-Merkez was severely damaged, even if the PGA values were lower than those of a number of Hatay and Kahramanmaras stations.

It serves as a foundation for understanding the seismic activity that is unique to Adiyaman. This information goes beyond PGA stats and is essential to comprehending the broader factors that influenced the structural flaws in the area. The potential danger of falling objects is one of the main risks that people in the streets faced during the two strong earthquakes and the ensuing aftershocks. When the ground shakes and buildings experience structural stress, bricks, glass, furniture, and other debris can break loose and fall from heights, posing a serious risk to people (Ivanov & Chow, 2023).

4.2 Data Collection and Analysis

Primarily, the aim was to detect fully collapsed structures on a post-earthquake high-resolution satellite picture and comparing it with the pre-earthquake satellite pictures of the buildings in Antakya and Kahramanmaras. The purpose of the experiment was also to determine the extent of building damage shown in these satellite photos (Saito et al., 2004). Satellite images

taken before and after the earthquake were collected (see Figure 11). They were imported into ArcGIS. An area with the largest concentration of buildings was identified as the study area.

Figure 11. The satellite images taken before and after the earthquake (Maxar Technologies)

All buildings that were in this area were annotated both in images before and after the earthquake. They help to better see all the buildings, roads and overall population density. These maps will depict the blocked road networks (rubble areas) thereby helping in finding the closest shelter or facility during the natural disaster.

Using network analysis in ArcGIS software, homeowners may run evacuation simulations by using the road network to get to the closest shelter depending on varying earthquake intensities. Additionally, residents can examine the accessibility of shelters from their homes. This approach was described in a paper that the Architecture Institute of Japan (AIJISA) Symposium on Computer Technology of Information, System, and Applications published. When comparing two evacuation instances, three factors are taken into account: the overall evacuation distances from evacuees' homes to main shelters; the four distance groups of 2km service areas: 0-500m, 500-1000m, 1000-2000m, and over 2000m; and the supply-to-demand ratio (SDR ratio) of each main shelter. The positions of roadblocks and network analysis data are utilized to simulate the evacuation of inhabitants to shelters (Nguyen, 2018).

Chapter 5 - Results

5.1 Dataset

Study aims to identify collapsed buildings from the satellite images using deep learning techniques. Satellite images of cities Antakya, Kahramanmaras and Adiyaman were collected which were influenced by 7.8 magnitude eartquake happened in Turkey in 2023. The images cover different levels of damage but the focus was on collapsed buildings area. Therefore only those areas were annotated in ArcGIS. Following Figures show pre- and post-earthquake images for all 3 cities that are considered in this study.

a) b)

Figure 13. Satellite imagery of a) pre-earthquake and b) post-earthquake for Antakya

a) b)

Figure 14. Satellite imagery of a) pre-earthquake and b) post-earthquake for Kahramanmaras

a) b)

Figure 15. Satellite imagery of a) pre-earthquake and b) post-earthquake for Adiyaman

The border lines of rubbles (or collapsed building areas) were marked using Polygon function in ArcGIS as in Figure below:

Figure 16. Annotated rubbles in ArcGIS

Satellite imagery for cities Antakya and Kahramanmaras were used to training the AI, whereas Adiyaman was saved till later to compare manual and automatic detection of the rubbles.

Using the ArcGIS function the images were converted to the black and white format, the former indicating the surroundings and the latter showing the rubble area and are called masks.

5.2 Data Augmentation

The process of data augmentation is done to increase the amount of dataset using number of alterations (Amirgan & Erener, 2024). This is a regularization approach that adds more

invariant cases by artificially inflating the data-set via label preserving changes. Both geometric and photometric modifications make up this augmentation system to make the CNN invariant to changes in location and orientation, geometric transformations modify the image's shape (Taylor & Nitschke, 2018). This study incorporates horizontal flip, vertical flip, random rotate 90, random gamma, grid distortion, random brightness contrast, median blur, gauss noise using Python software.

5.3 Semantic Segmentation

Before selecting the proper model for the data segmentation several models were accessed. Hacıefendioˇglu et al. (2018) have evaluated the the performance of four different architectures—U-Net, LinkNet, FPN, and PSPNet using a number of performance metrics, including accuracy, precision, recall, F1 score, specificity, AUC, and IoU. The study used satellite imagery from the south and southeast of Turkey, which includes the eleven provinces most affected by the Mw 7.7 Pazarcık (Kahramanmaras) and Mw 7.6 Elbistan (Kahramanmaras) earthquakes. The results indicated that FPN and U-Net were the top-performing models based on the relevant performance criterion. FPN achieved the highest accuracy, specificity, and precision scores, whereas U-Net achieved the best recall and F1 score values. The study of the training and validation accuracy and loss curves showed that all four models had an accuracy value of above 96%. The FPN model outperformed the others in accurately segmenting images with a low loss value.

Deep learning-based semantic segmentation algorithms were used by Amirgan & Erener (2024) to autonomously extract buildings from a remote sensing picture of a sample area that contained a small portion of Istanbul. First, in this context, the concepts of fully convolutional networks, semantic segmentation inference, and publicly available open source construction datasets were explored. Extremely high quality Pleiades satellite pictures were used to produce the project's IST building dataset, which includes samples from five distinct building type classes. This dataset was then used to train the UNet and UNet++ architectures for segmentation creation. Based on their kinds, the segmentation success of the training models and the construction classes was compared. According to experimental data, the Industrial class's segmentation success IOU metric was 0.9167 and 0.9150, the Adjacent class's was 0.8124 and

0.8175, the Housing-Villa class's was 0.8459 and 0.8446, the Slum class's was 0.7629 and 0.7477, and the Other class' was 0.6697 and 0.6140.

In the study done Pan et al. (2020), a paradigm for mapping urban villages based on the U-net deep learning architecture was proposed. The study area is located in Guangzhou City, China. The building boundary vector file and the Worldview satellite image with eight pan-sharpened bands at a spatial resolution of 0.5 m were used for the study's goals. Eleven urban village locales are included in this Worldview image. The deep neural network model was trained and tested using the selected six and four urban village sites, respectively. Models for segmentation and categorization of buildings were trained and assessed. The findings showed that the U-net model's overall accuracy for constructing segmentation was over 86%, and for classification, it was over 83%. The F1-scores for classification and segmentation ranged from 0.63 to 0.88 and 0.9 to 0.98, respectively. The Interaction over Union was above 90% for segmentation and 86% for classification. The superiority of the deep learning method has been demonstrated through comparisons with Random Forest and object-based image analysis.

Other studies are concluded in the following Table:

Table 1. Data Segmentation comparison

Paper Name	Dataset labels	# images	Model	Model input	Data augmentation	Results
Automatic Detection of Collapsed Buildings after the 6 February 2023 Türkiye Earthquakes Using Post-Disaster Satellite Images with Deep Learning-Based Semantic Segmentation Models	collapsed buildings are masked	377 (train: 302, val: 75)	U-Net LinkNet FPN PSPNet	512x512	No	FPN (best accuracy) & U-Net (best IoU) A pre-trained ImageNet backbone improves the performance.
Semantic segmentation of	5 different	Train: 1470	U-Net & U-Net++	256x256	Horizontal flip Affine	UNET and UNet++

satellite images with different building types using deep learning methods	building type classes	Val: 420	Backbone encoder: “Efficient net-b0”		transformation Perspective transformation Brightness/contrast/color operations Image blurring and sharpening Gaussian noise Random cuts	achieved IoU of 0.9167 and 0.9150 for Industrial class, 0.8124 and 0.8175 for Adjacent class, 0.8459 and 0.8446 for Housing-Villa class, 0.7629 and 0.7477 for Slum class, 0.6697 and 0.6140 for Other class
Deep Learning Segmentation and Classification for Urban Village Using a Worldview Satellite Image Based on U-Net	4 categories were used: “Old house,” “Old factory,” “Iron roof building,” and “New building.”	10,000 (train: val = 6:4	U-Net structure	256x256	Rotation Mirroring Brightness enhancement Adding noise points	Over 93% overall accuracy for training sites and over 86% accuracy for test sites
Comparing the robustness of U-Net, LinkNet, and FPN towards label noise for refugee dwelling extraction from satellite imagery	two binary classes: “structures” and “background”	Train: 8286 Val: 921 Testing: 210	tested multiple models U-Net, LinkNet, and FPN with various backbones	128x128	No	U-Net model with EfficientNet-B0 backbone encoder outperform others for satellite image segmentation

Hybrid U-Net: Semantic segmentation of high-resolution satellite images to detect war destruction	2 classes: “destroyed areas” and “background”	252 images: 60% training, 10% validation, 30% testing.	Hybrid U-Net architecture, which extends the U-Net model by adding multiscale skip connections.	1248x1248	No	Mean Dice Coefficient (MDC): 76.10% Overall Accuracy (OA): 92.38%
Satellite Image Segmentation for Building Detection using U-net	"building" vs. "background"	2129 training 456 validation	U-Net	224x224 pixels	Shifting Fipping Rotation	Dice Coefficient: 0.75 Jaccard Index (IoU): 0.60

According to the literature review, the U-Net and U-Net++ models showed the best performance so it was decided to utilize it. It is the effective with small datasets as it works well even with limited annotated data. It has precise localization and combines high-level (coarse) and low-level (fine) features. Also, it is easy to train for pixel-wise classification tasks and it handles different object sizes and shapes well. Below the architecture of the U-Net is depicted that uses encoder-decoder architecture with skip connections:

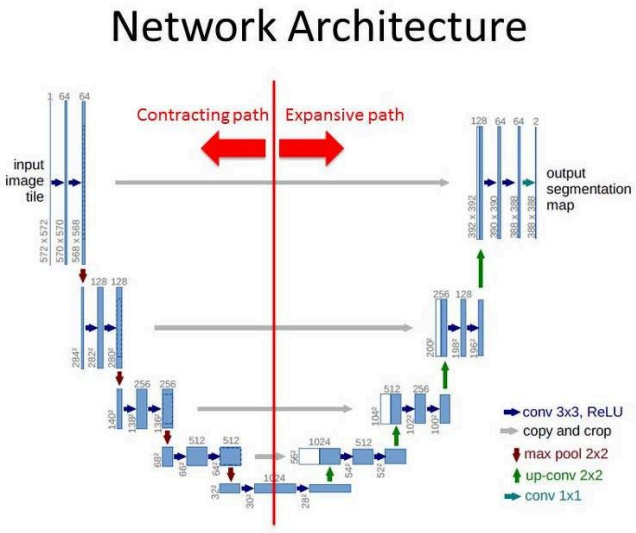

Figure 17. U-Net Model Architecture

Input image size was 256x256 for all images. For the evaluation of the accuracy dice score was used which measures the overlap between actual and predicted masks to see how well the predicted segmentation matches the ground truth.

5.4 Results and Discussion

Images were tested in different ways to improve the accuracy of the model. In total there were 4 training experiments.

5.4.1. Training experiment 1

First, the model configurations are introduced:

Input image size: 256x256. It is a uniform size of images, if there is a need to make the masks clearer then the size will be increased to 512x512 or even higher.

Shift in Step Size: 256 pixels. This parameter is usually equal to input image size as it helps to avoid overlapping. However, it is often time-consuming and some U-Net systems do not utilize that.

Number of epochs: 30. The most optimal number that provides image segmentation without overfitting.

Batch size: 8. The parameter that balances training stability and memory use.

Loss: DiceLoss. It is an assessment index based on which overlap between original mask and predicted mask is optimized.

Optimizer: Adam.

Learning Rate: 1e-4. This parameter paired with Adam optimizer ensures consistent training.

Accuracy Metric: Dice score. It compares the possible and ground truth segmentations so it is widely used metric.

Dataset (Antakya):

Overall number of images: 754

Training set: 603 images

Validation set: 75 images

Test set: 76 images

Model configurations:

Input image size: 256x256

Shifting step size: 256 pixels

Number of epochs: 30

Batch size: 8

Loss: DiceLoss

Optimizer: Adam

Learning rate = 1e-4

Accuracy Metric: Dice score

Table 2. Experiment 1 results

Segmentation Model	**Backbone encoder**	**Train Accuracy**	**Val Accuracy**	**Test Accuracy**
UNet	EfficientNet-b0	0.8974	0.6806	**0.7337**
UNet++	ResNet-50	0.9329	0.6946	**0.737**

Two models were utilized including UNet and it better version UNet++. Also, these models work based on encoder and decoder concept using backbones. During the first trial, only Antakya satellite images were analyzed: it consisted of 754 images and was divided into 3 categories (training, validation and testing). For training set 603 images, for validation 75, and test set 76 images. 2 backbone encoders EfficientNet-b0 and ResNet-50 showed somewhat similar results. However, ResNet-50 depicted better results in every stage. The first experiment proved that the model is working.

5.4.2. Training experiment 2

As the first experiment was successful, for the second experiment it was decided to increase the number of images and all 4 images of Antakya were there. And the patch size remained the same with the resolution of 17408 x 17408, also shifting window step size was decreased. At this stage the number of images for training, validating and testing were much higher (5x) from first experiment due to the bigger number of images. Also, four type of data augmentation were applied to the images: horizontal flip, vertical flip, random rotate 90, random gamma. This added up to the number of images and masks. Moreover, pretrained weights were applied to the images (Imagenet). Basically, models with pretrained weights showed better

results than without. Training accuracy was >0.97 whereas validation accuracy was >0.60, and as far as for the test accuracy the numbers exceeded 0.76. It is already promising results.

Dataset (Antakya):

4 satellite images with corresponding segmentation masks (031133023321, 031133023302, 031133023303, 031133023320)

Resolution for all images: 17408 x 17408

Table 3. Data Preprocessing

Patch size: 256x256 Shifting window step size: 100 pixels Number of patches that contain segmentation in each image: - 031133023321 is: 165 (test) - 031133023302 is: 2784 (train) - 031133023303 is: 1401 (train) - 031133023320 is: 771 (val)	Finally: - Train: 4185 - Val: 771 - Test: 165	Augmentations (randomly apply one of): - HorizontalFlip - VerticalFlip - RandomRotate90 - RandomGamma

Table 4. Experiment 2 results

Model	**Backbone encoder**	**Pretrained weights**	**Train (aug 2x)**	**Val**	**Test**	**Train Accuracy**	**Val Accuracy**	**Test Accuracy**
UNet	EfficientNet-b0	Imagenet	8370	771	165	0.9739	0.6034	**0.7807**
UNet++	ResNet-50	Imagenet	8370	771	165	0.9745	0.6002	**0.7607**
UNet	EfficientNet-b0	None	8370	771	165	0.8910	0.4780	**0.5701**

UNet++	ResNet-50	None	8370	771	165	0.9366	0.5166	**0.7142**

5.4.3. Training experiment 3

The best results were chosen from experiment 2 and the number of images were increased to test whether the model will work in case of large amount of data. Also, the background image patches were added to allow model recognize not only rubbles bus also "not affected" areas. Therefore, dataset was drastically increased to 24925 due to that the augmentations rised 5 times and also 20% of background images were added to the training dataset. Also, all test sets used all patch images. Number of augmentations exceeded 8 and every image was randomly applied one of them. Training accuracy was equal to 0.97, validation accuracy 0.63. Testing accuracy using all images was equal to 0.70 whereas for the sample it was 0.76. When experiment shows the best training results, it is unlikely that other parts will have the same results because it usually have trouble generalizing to new data.

The model proved that it works well in conditions of increased number of patches and background images.

Table 5. Dataset for the 3rd experiment

Dataset	Augmentations (randomly apply one of):
- Train: augmentation 5x + 20% background images - Val: + 20% background images - Test: all patch images (29k)	- HorizontalFlip - VerticalFlip - RandomRotate90 - RandomGamma - GridDistortion - RandomBrightnessContrast - MedianBlur - GaussNoise

Table 6. Experiment 3 results

Model	**Backbone encoder**	**Pretrained weights**	**Train images**	**Val images**	**Test images**	**Train Accurac**	**Val Accurac**	**Test Accuracy**	**Test Accuracy**

						y	y	(all imgs)	(165 imgs)
UNet	EfficientNet-b0	Imagenet	24925	921	29584	0.9686	0.6251	0.7040	**0.7596**

5.4.4. Training experiment 4

Next, Kahramanmaras data was added. For the training set 2 images of Antakya and 1 image of Kahramanmaras were utilized and on top of that 5 times augmentation was applied adding 20% of background images. For the validation part, equal number of images were there and only 3x augmentation used with 20% of background images. For the testing there were no modifications. From the previous stage, it was decided to utilized pretrained weights because it showed better accuracy. Backbone encoder ResNet-50 depicted slightly better outcomes than ResNet-50.

Testing data accuracy decreased because the features differ for two cities. It was because of mountainous terrain of Kahramanmaras city. The model labels them as a rubble.

Table 7. Combined Dataset (Antakya+Kahramanmaras)

Split	**Number of images used**		**Number of patches**		**Augmentation**	**Background patches (no segmentation)**	**Final**
	Antakya	Kahramanmaras	Antakya	Kahramanmaras			
Train	2	1	4185	1679	5x	20%	33320
Val	1	1	771	198	3x	20%	3477
Test	1	1	165	347	-	0%	512
Test all	1	1	29584	29584	-	100%	59168

Table 6. Experiment 4 results

Model	**Backbone encoder**	**Pretrained weights**	**Train**	**Val**	**Test (512)**	**Test (all)**

UNet	EfficientNet-b0	Imagenet	**0.9599**	**0.6135**	**0.4673**	**0.5216**
UNet++	ResNet-50	ImageNet	0.9654	0.5899	0.4909	**0.6734**

5.4.5. Training experiment 5

The last experiment involves combined data and so far it is the best results. For training it is 0.93, validation 0.69 and test set 0.50.

Experiments (2 cities data):

- Different patch sizes: 256x256, 512x512
- Different shifting window step sizes: 128, 192, 256 pixels
- Added more augmentation methods
- Decreased background patches percentage to 10%
- Experimented with different model & training hyperparameters

Best parameters:

- **Dataset:** patch size=256x256, step size=192, adding more augmentation functions, augmentation=8x for the train set, adding 10% background images
- **Training hyperparameters:** batch=8, optimizer weight decay, epoch=30, sigmoid activation
- **Model parameters:** adding dropout, decreasing model complexity by reducing size of decoder channels & encoder depth

Table 7. Experiment 5 results

Model parameters			**Combined Data**			**Antakya**		**Kahramanmaras**	
Model	Backbone encoder	Pretrained weights	Train aug (13976 imgs)	Val (298 imgs)	Test (142)	Val (219)	Test (46)	Val (54)	Test (96)
UNet	EfficientNet-b0	Imagenet	**0.9319**	**0.6913**	**0.4982**	0.636	0.7928	0.7319	0.3510

Chapter 6 - Conclusions

6.1 Conclusion

This study uses ArcGIS and AI to detect rubbles that cause road blockages after the earthquake. Therefore this work addresses a major problem in disaster management. The methodology of this study suggests using the high resolution satellite images before and after the earthquake, annotating the rubbles on them and using it further as an input to deep data learning for AI purposes. For this part, the model utilizes the semantic segmentation model like UNet and UNet++ to recognize the rubbles automatically. Using ArcGIS the affected areas after the earthquakes can be visually depicted.

For now data was trained on the base of two cities: Antakya and Kahramanmaras. Using the backbone encoder, and pretrained weights also applying the data augmentation techniques the number of images and data were increased drastically. It provided better results and accuracy for future use. The next stage will involve testing the Adiyaman data and comparing the originally annotated and automatically annotated data. It will demonstrate whether the model can provide high accuracy and is safe to future use.

With the help of ArcGIS and AI, the model showed a detection accuracy of 0.9319 for the training set, 0.6913 for the validation set, and 0.4982 for the test set.

Studies show that AI based models are more effective, efficient and have more accuracy over traditional and probabilistic methods as the latter involves a set of parameters to consider and long equations to calculate the road blockage. And it does not align with the main aim of this research which is integration of real time detection of rubbles.

Still there are limitations which include the lack of satellite images as there are only images only for three cities. In addition, there are potential for overfitting. By addressing these problems, there is a potential to make the model better.

Despite the drawbacks, it is a significant step forward in the development of disaster management. The work demonstates the main problems of emergency responce in urban resilience.

6.2 Limitations of the study

The research has its own limitations. The first challenge that was faced during the initial stage was to find satellite images in high resolution. For example, satellite images of Kahramanmaras have better quality over Antakya and Adiyaman. The latter ones have questionable quality which made the rubble identification process more difficult. Some other cities' satellite images are even costly so you need to buy it in order to use it as a dataset. Moreover, the fact that only three cities were analyzed is a major drawback because it is not sufficient to train the model on an international level. The number of images should be more and diverse to increase the accuracy of the model as well as the generalizability. It is due to the fact that the architectural layout of the cities from various countries may differ.

The current model's training set pose an issue in terms of overfitting. The model can perform well in previously trained data but when it comes to the new set of datasets it crashes.

Now system can not predicts the road blockages in real time since it uses satellite images from the archive taken before and after the earthquake. If emergency happens system might not be able to react quickly without the images. It is due to the fact that the satellite images cannot be received immediately after the earthquake. Therefore, it will be effective to use sensors or drones.

As it was written before, only three cities were considered in this particular study which do not reflect the circumstances in the rest of the countries.

Also, even though it will prove itself as a working instrument it will take a big amount of time to just implement it. It is due to the fact that it needs to be checked for alignment to regulations and policies.

And one more time, over inhabitated areas with high density may pose difficulties in identifying the rubbles because of the image distortion.

6.3 Future Work

6.3.1. Comparison of manual and automatic annotation

Adiyaman was only marked and reserved for testing, but Antakya and Kahramanmaraş were annotated and trained using deep learning techniques. Adıyaman will be used as a test site in the following phase to assess the trained model's ability to recognize rubble on satellite images

on its own. After processing the images, the algorithm will produce predictions that will be contrasted with the previously made manual annotations. This comparison will aid in evaluating the model's accuracy and dependability.

The build framework will be effective if it matches manual annotation done in ArcGIS Pro. The research will further expand by adding a new city in order to improve the testing process and try variable inputs. To test whether this model can ran smoothly in a new setting the city will be chosen from outside of Turkey. It can contribute to theat the model will be used internationally so that is why itwill be improved by adding new sceneries, building designs and urban layouts. Perhaps, it will be decided that there is a need in training data.

The whole methodology of this study is based on 3 cities of Turkey so it is important to test it also in unfamiliar settings. If it is successful, then it will be used as one of emergency response tools.

Manual annotations are important part of the methodology, however in terms of time it is not very efficient. During emergencies people would not be able to receive quick results. That is why it is better to train the AI which will analyze the data in matter of seconds and will provide plans in case of natural disasters.

It should be taken into account that this model can be modenized and altered to fit other events or natural disasters. Now, when automatic systems with human intelligence are working in tandem with othher colleagues, it will save much more time and other resources.

6.3.2. Addition of new study area

This study's inclusion of Morocco is a way to see how well the model performs in various geographical areas. Much damage was inflicted by the recent Moroccan earthquake, particularly in towns like Marrakesh and the High Atlas Mountains. These places present a new challenge for the model since they differ greatly from those that have already been researched in Turkey.

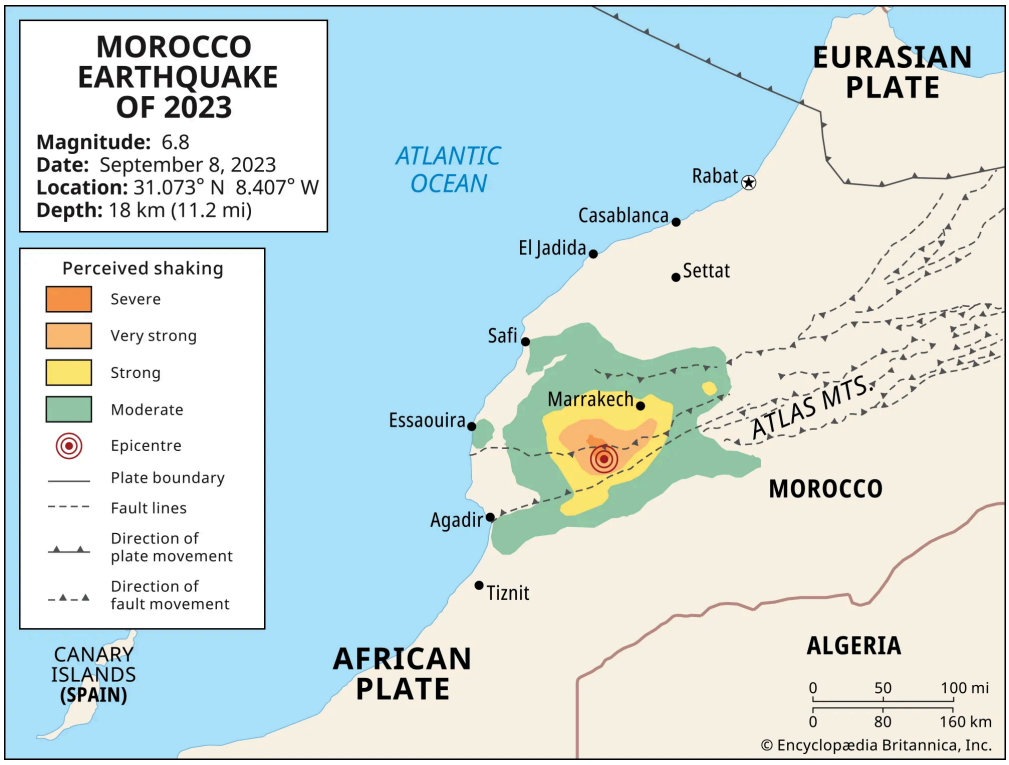

Figure 18. Morocco seismicity

Native Ima-zighen people make up the majority of the Al-Haouz area, which was hit by an earthquake in September 2023. The area is situated in the High Atlas, the Atlas Mountain range's highest point. With more than 1,000 fatalities and traffic jams, the earthquake left chaos and destruction in its wake. In order to rescue people who were buried under the debris, locals had to help one another. While Moroccans living overseas combined their resources, civil society organizations engaged their networks (Errazzouki, 2024).

An earthquake of a magnitude of 6.8 struck Morocco on September 9, 2023, close to the Al Haouz neighborhood southwest of Marrakech. The epicenter was in the commune of Ighil, 71.8 kilometers southwest of Marrakech. The earthquake caused almost 50,000 residential buildings to fall, killed 2901 people, and injured 5530 others, including 1404 badly injured. It was the most devastating earthquake to hit Morocco since at least 1960 and the second worst worldwide in 2023, behind the earthquakes in Syria and Turkey. Morocco has been actively helping rescue efforts, and the Kingdom of Morocco has seen incredible commitment from Qatar, Spain, the United Arab Emirates, and the United Kingdom (Achbani, 2024).

6.3.3. Closest Network Facility Analysis (CFNA)

During and after an earthquake, people are forced to leave the buildings they are in and seek out open areas in order to feel safe and secure. Since these areas meet people's needs for housing, safety, and escape from seismic disasters, they should be more common and of greater quality in addition to the social, psychological, and economic advantages they provide to the city. The open areas scattered across the city have been designated as disaster and emergency meeting locations because they match some of the requirements listed in this study (Onay, 2024).

Using the Closest Facility feature in Network Analysis in ArcGIS Pro is aimed to determine the most efficient routes. In the first or initial scenario, the network investigation is going to be conducted normally, without any obstacles. This program should provide the fastest routes to get the individuals gathered at the incident sites to the designated EGAs.

In a second or subsequent scenario, concept of rubbles will be introcuded, and the regions that were closed will be indicated using polygonal annotations. The concept of traffic obstacle originated from the debris left over after buildings fell during or after earthquakes. The obstructions caused by this rubble interfere with traffic flow. Building rubble sites are identified, and the relevant roads will be strategically closed to allow for effective traffic management and regulation. If the debris blocked a road portion in our situation, it will be deemed completely inaccessible. The route analysis in the second scenario will show alternative paths to the safety zones to take into consideration the presence of barriers.

The research will be extended to incorporate emergency response measures in the third scenario, which comprised vehicles from beyond the impacted region, such as fire vehicles and medical units. It is simulated that these vehicles will go toward the earthquake-affected areas via a main highway. The primary objective is to determine the most efficient routes for these rescue vehicles to swiftly reach the designated zones.

6.3.4. Model Evaluation and Validation

The study incorporates the dice score when it comes to evaluation of the model. However, it is insufficient to access the whole picture. Literature review showed that other studies have been utilizing the metrics such as Sensitivity, Precision and F-1 score.

Dice score compares the possible and ground truth segmentations. Sensitivity measures the part of the segmentation that is actually correctly identified by the model. Precision is the metric that measures the proportion of the positives throughout all the instances.

Finally, F-1 score is the mean of precision and sensitivity:

$$Dice\ Coefficient\ (DC) = \frac{2 \times TP}{2TP + FP + FN}$$

$$Recall\ (R) = Sensitivity\ (TPR) = \frac{TP}{TP + FN}$$

$$Precision\ (P) = \frac{TP}{TP + FP}$$

$$F1 - Score = 2 \times \frac{P \times R}{P + R}$$

All these metrics will add to the final findings so that the results become more reliable and accurate.

References

Achbani, A., Bouchriti, Y., Sine, H., Kharbach, A., Boukrim, M., Rida, J., ... & Sine, H. (2024). Key Takeaways From the Al Haouz Earthquake, Morocco, 2023. *Disaster medicine and public health preparedness, 18*, e88.

Amirgan, B., & Erener, A. (2024). Semantic segmentation of satellite images with different building types using deep learning methods. *Remote Sensing Applications: Society and Environment, 34*, 101176.

Anbazhagan, P., Srinivas, S., & Chandran, D. (2012). Classification of road damage due to earthquakes. *Natural hazards, 60*, 425-460.

Argyroudis, S., Pitilakis, K., & Anastasiadis, A. (2005, May). Roadway network seismic risk analysis in urban areas: The case of Thessaloniki-Greece. In Proceedings of the Geoline Conference, Lyon, France.

Caiado, G., Oliveira, C., Ferreira, M. A., & Sá, F. (2012). Assessing urban road network seismic vulnerability: An integrated approach. *Proceedings of the 15WCEE, Lisbon, Portugal,* 24-28.

Cheloni, D., Famiglietti, N. A., Tolomei, C., Caputo, R., & Vicari, A. (2024). The 8 September 2023, MW 6.8, Morocco earthquake: A deep transpressive faulting along the active high Atlas mountain belt. *Geophysical Research Letters, 51*(2), e2023GL106992.

Chhor, G., Aramburu, C. B., & Bougdal-Lambert, I. (2017). Satellite image segmentation for building detection using U-Net. Web: http://cs229. Stanford. edu/proj2017/final-reports/5243715. Pdf.

Davidson, R. A., & Shah, H. C. (1997). An urban earthquake disaster risk index. Report 121. *Blume Earthquake Engineering Center, Standford*, USA.

Eelbode, T., Sinonquel, P., Maes, F., & Bisschops, R. (2021). Pitfalls in training and validation of deep learning systems. *Best Practice & Research Clinical Gastroenterology, 52*, 101712.

Errazzouki, S. (2024). Between rubble and rage: reflections on the earthquake in Morocco and its aftermath. *The Journal of North African Studies, 29*(2), 197-205.

Feizizadeh, B., Adabikhosh, S. J., & Panahi, S. (2023). A Scenario-Based and Game-Based

Geographical Information System (GIS) Approach for Earthquake Disaster Simulation and Crisis Mitigation. *Sustainability, 15*(14), 11131.

Franchin, P., Cavalieri, F., Pinto, P. E., Lupoi, A., Vanzi, I., Gehl, P., ... & Kakderi, K. (2011). General methodology for systemic vulnerability assessment. P*roject SYNER-G, Reference Report, 1*.

Gao, Y., Lang, S., Tiede, D., Gella, G. W., & Wendt, L. (2022, September). Comparing the robustness of U-Net, LinkNet, and FPN towards label noise for refugee dwelling extraction from satellite imagery. In 2022 IEEE Global Humanitarian Technology Conference (GHTC) (pp. 88-94). IEEE.

General Directorate of Disaster Afairs, Ministry of Public Works and Settlement of Turkey, GDDA (2019) Seismic Hazard Map of Turkey, Ankara

Giwa, Y. A., & Fakokunde, A. (2024). PREDICTIVE MODELING FOR DISASTER MANAGEMENT.

Goretti, A., Sarli, V. (2006). Road network and damaged buildings in urban areas: Short and long-term interaction. *Bulletin of Earthquake Engineering 4*(2):159-175, DOI: 10.1007/s10518-006-9004-3

Hansapinyo, C., Latcharote, P., & Limkatanyu, S. (2020). Seismic building damage prediction from GIS-based building data using artificial intelligence system. *Frontiers in Built Environment*, *6*. https://doi.org/10.3389/fbuil.2020.576919

Hacıefendioğlu, K., Başağa, H. B., Kahya, V., Özgan, K., & Altunışık, A. C. (2024). Automatic Detection of Collapsed Buildings after the 6 February 2023 Türkiye Earthquakes Using Post-Disaster Satellite Images with Deep Learning-Based Semantic Segmentation Models. *Buildings, 14*(3), 582.

Hassanzadeh, R., Nedović-Budić, Z., Razavi, A. A., Norouzzadeh, M., & Hodhodkian, H. (2013). Interactive approach for GIS-based earthquake scenario development and resource estimation (Karmania hazard model). *Computers & geosciences, 51*, 324-338.

Hirokawa, N., & Osaragi, T. (2016). Earthquake disaster simulation system: Integration of models for building collapse, road blockage, and fire spread. *Journal of Disaster Research, 11*(2), 175-187.

Hosseini, Y., Mohammadi, R. K., & Yang, T. Y. (2023). Resource-based seismic resilience optimization of the blocked urban road network in emergency response phase considering

uncertainties. *International Journal of Disaster Risk Reduction, 85*, 103496.

Hosseini, Y., Mohammadi, R. K., & Yang, T. Y. (2024). A comprehensive approach in post-earthquake blockage prediction of urban road network and emergency resilience optimization. *Reliability Engineering & System Safety, 244*, 109887.

İnce, Y., & Kurnaz, T. F. (2018). Probabilistic seismic hazard analysis of Kahramanmaras Province, Turkey. *Arab J Geosci, 11*(5), 97.

Işık, E., Avcil, F., İzol, R., Büyüksaraç, A., Bilgin, H., Harirchian, E., & Arkan, E. (2024). Field Reconnaissance and Earthquake Vulnerability of the RC Buildings in Adıyaman during 2023 Türkiye Earthquakes. Applied Sciences, 14(7), 2860.

Ito, E., Kawase, H., Matsushima, S., & Hatayama, M. (2020). Tsunami evacuation simulation considering road blockage by collapsed buildings evaluated from predicted strong ground motion. *Natural Hazards, 101*, 959-980.

Ivanov, M. L., & Chow, W. K. (2023, December). Structural damage observed in reinforced concrete buildings in Adiyaman during the 2023 Turkiye Kahramanmaras Earthquakes. *In Structures* (Vol. 58, p. 105578). Elsevier.

Kalantar, B., Ueda, N., Al-Najjar, H. A. H., & Halin, A. A. (2020). Assessment of convolutional neural network architectures for earthquake-induced building damage detection based on pre- and post-event orthophoto images. *Remote Sensing*, *12*(21), 3529. https://doi.org/10.3390/rs12213529

Kawashima, K., & Matsuzaki, H. (2012). Damage of road bridges by 2011 Great East Japan (Tohoku) earthquake. *In Proc., 15th World Conf. of Earthquake Engineering* (pp. 24-28).

Krawinkler, H., & Zareian, F. (2007). Prediction of collapse—How realistic and practical is it, and what can we learn from it?. *The Structural Design of Tall and Special Buildings, 16*(5), 633-653.

Liu, C., Sepasgozar, S. M., Zhang, Q., & Ge, L. (2022). A novel attention-based deep learning method for post-disaster building damage classification. *Expert Systems with Applications, 202*, 117268.

Lo, IT., Lin, CY., Yang, CT. et al. Assessing the Blockage Risk of Disaster-Relief Road for a Large-Scale Earthquake. *KSCE J Civ Eng 24*, 3820–3834 (2020). https://doi.org/10.1007/s12205-020-0340-7

Mangalathu, S., Sun, H., Nweke, C. C., Yi, Z., & Burton, H. V. (2020). Classifying earthquake damage to buildings using machine learning. *Earthquake Spectra, 36*(1), 183-208.

Matin, S. S., & Pradhan, B. (2021). Earthquake-induced building-damage mapping using Explainable AI (XAI). *Sensors, 21*(13), 4489.

Mertol, H. C., Tunç, G., Akış, T., Kantekin, Y., & Aydın, İ. C. (2023). Investigation of RC buildings after 6 February 2023, Kahramanmaraş, Türkiye earthquakes. *Buildings, 13*(7), 1789.

Nabiee, S., Harding, M., Hersh, J., & Bagherzadeh, N. (2022). Hybrid U-Net: Semantic segmentation of high-resolution satellite images to detect war destruction. *Machine Learning with Applications, 9*, 100381.

Nguyen, D. T. (2018). GIS-based Simulation for Evacuation Planning Support in Case of Earthquake (Doctoral dissertation, Kanazawa University).

Nguyen, D. T., Shen, Z. J., Truong, M. H., & Sugihara, K. (2021). Improvement of evacuation modeling by considering road blockade in the case of an earthquake: A case study of Daitoku school district, Kanazawa city, Japan. *Sustainability, 13*(5), 2637.

Onay, B. (2024). A study on the adequacy of gathering areas as urban spaces. *Artvin Çoruh Üniversitesi Orman Fakültesi Dergisi, 25*(1), 95-103.

Över, S., Büyüksaraç, A., Bekta, Ö., & Filazi, A. (2011). Assessment of potential seismic hazard and site effect in Antakya (Hatay Province), SE Turkey. *Environmental Earth Sciences, 62*, 313-326.

Özşahin, E., & Değerliyurt, M. (2013). Modeling of seismic hazard risk analysis in Antakya (Hatay, South Turkey) by using GIS. *International Journal of Innovative Environmental Studies Research, 1*(3), 31-54.

Pan, Z., Xu, J., Guo, Y., Hu, Y., & Wang, G. (2020). Deep learning segmentation and classification for urban village using a worldview satellite image based on U-Net. *Remote Sensing, 12*(10), 1574.

Ranjbar, H. R., Dehghani, H., Ardalan, A. R. A., & Saradjian, M. R. (2017). A GIS-based approach for earthquake loss estimation based on the immediate extraction of damaged buildings. *Geomatics, Natural Hazards and Risk, 8*(2), 772-791.

Saito, K., Spence, R. J., Going, C., & Markus, M. (2004). Using high-resolution satellite images for post-earthquake building damage assessment: a study following the 26 January 2001 Gujarat earthquake. *Earthquake spectra, 20*(1), 145-169.

Shahi, K. (2024). Remote Sensing and Machine Learning for the Detection and Segmentation of Landslides in Nepal (Master's thesis, Universidade NOVA de Lisboa (Portugal)).

Spence, R., So, E., Ameri, G., Akinci, A., Cocco, M., Cultrera, G., ... & Demircioglu, M. (2007). Earthquake disaster scenario prediction and loss modelling for urban areas.

Sun, W., Bocchini, P., & Davison, B. D. (2020). Applications of artificial intelligence for disaster management. *Natural Hazards, 103*(3), 2631-2689.

Taylor, L., & Nitschke, G. (2018, November). Improving deep learning with generic data augmentation. In 2018 IEEE symposium series on computational intelligence (SSCI) (pp. 1542-1547). IEEE.

Toma-Danila, D. (2018). A GIS framework for evaluating the implications of urban road network failure due to earthquakes: Bucharest (Romania) case study. *Natural Hazards, 93*(Suppl 1), 97-111.

Tong, X., Hong, Z., Liu, S., Zhang, X., Xie, H., Li, Z., Yang, S., Wang, W., & Bao, F. (2012). Building-damage detection using pre- and post-seismic high-resolution satellite stereo imagery: A case study of the May 2008 Wenchuan earthquake. *ISPRS Journal of Photogrammetry and Remote Sensing: Official Publication of the International Society for Photogrammetry and Remote Sensing (ISPRS)*, *68*, 13–27. https://doi.org/10.1016/j.isprsjprs.2011.12.004

Tung, P. T. (2004). Road vulnerability assessment for earthquakes. ITC-Faculty of Geo-Information Science and Earth Observation.

Yoshinari, N., Yamamoto, M., Tonegawa, R., Oyanagi, Y., & Ohuchi, A. (2017). Detecting collapsed buildings from image data for estimation of disaster debris. In IOP Conference Series: *Earth and Environmental Science (Vol. 61*, No. 1, p. 012163). IOP Publishing.

Vural, E. (2024). Assessment of Particle Matter Pollution during Post-Earthquake Debris Removal in Adiyaman City. *RIG, 33*.

Yu, Y. C., & Gardoni, P. (2022). Predicting road blockage due to building damage following

earthquakes. *Reliability Engineering & System Safety, 219*, 108220.

Yu, B., Xing, H., Yan, J., & Li, Y. (2024). Small-scale, large impact: utilizing machine learning to assess susceptibility to urban geological disasters—a case study of urban road collapses in Hangzhou. *Bulletin of Engineering Geology and the Environment, 83*(11), 1-19.

Zareian, F., Krawinkler, H., Ibarra, L., & Lignos, D. (2010). Basic concepts and performance measures in prediction of collapse of buildings under earthquake ground motions. *The Structural Design of Tall and Special Buildings*, *19*(1‐2), 167-181.

Zou, R., Liu, J., Pan, H., Tang, D., & Zhou, R. (2024). An Improved Instance Segmentation Method for Fast Assessment of Damaged Buildings Based on Post-Earthquake UAV Images. *Sensors, 24*(13), 4371.